



PEM Fuel Cell Pt/C Dissolution and Deposition in Nafion Electrolyte

Wu Bi,^{a,*} Gary E. Gray,^{b,**} and Thomas F. Fuller^{a,b,**}

^aSchool of Chemical and Biomolecular Engineering, and ^bCenter for Innovative Fuel Cell and Battery Technologies, Georgia Tech Research Institute, Georgia Institute of Technology, Atlanta, Georgia 30332, USA

Dissolution at the cathode and subsequent transport of platinum to the other cell components causes catalyst degradation in proton exchange membrane (PEM) fuel cells. Deposition of platinum in Nafion membrane was observed after potential cycling under hydrogen/air conditions. The deposited Pt formed a band in the ionomer, and a straightforward model was proposed to describe its location. The predicted position of the Pt band agreed with the experimental data. A simple scanning electron microscopy-energy dispersive spectroscopy analysis was used to estimate that ~13% of the platinum initially in the cathode was transported into the membrane following 3000 potential cycles.

© 2007 The Electrochemical Society. [DOI: 10.1149/1.2712796] All rights reserved.

Manuscript submitted September 6, 2006; revised manuscript received January 9, 2007. Available electronically March 7, 2007.

Carbon-supported platinum is the most common and effective catalyst for the oxygen reduction reaction (ORR) in proton exchange membrane (PEM) fuel cells. However, platinum has a small but finite solubility¹ in the acidic Nafion ionomer matrix given the high potential and oxidizing environment at the cathode. This solubility leads to one of the Pt catalyst degradation processes. Specifically, under accelerated degradation tests that include potential cycling dissolution was identified²⁻⁴ and subsequently simulated.^{5,6} Soluble Pt ions that are formed at the cathode can be transported to the other fuel cell regions, such as the Nafion membrane, by diffusion, migration, and possibly convection. Ferreira observed that Pt migrated into the membrane and formed a Pt band after 2000 h of open-circuit operation on H₂ (anode gas)/air(cathode gas).⁷ We adopt the convention in this article of describing compositions by listing the anode gas followed by the cathode gas separated by a slash (/): anode gas/cathode gas.

Yasuda further studied Pt dissolution and deposition in membrane under different potential cycling conditions.⁸ Following N₂/N₂ potential cycling, in the absence of hydrogen, Pt ions were transported through membrane and plated on the negative carbon electrode. Yasuda also found a Pt band in the membrane after 500 H₂/air potential cycles; however, Pt only deposited at the membrane-cathode interface in the H₂/N₂ case. But in another study by Yu,⁹ a Pt band was observed in the membrane (~5 μm away from the cathode) after 2400 H₂/N₂ potential cycles.

In this study, the Pt deposition process was investigated under H₂/air and H₂/N₂ potential cycling conditions. Hydrogen and air crossover rates through Nafion membrane were measured. A simplified model describing the Pt-deposition process and the effects of hydrogen and air permeability is proposed. The model predicts the Pt band location in the membrane. The quantity of Pt metal removed from the cathode and transported into the membrane was estimated by scanning electron microscopy-energy dispersive spectroscopy (SEM-EDS) analyses.

Experimental

Commercial membrane electrolyte assemblies (MEAs) measuring 5 × 5 cm with gas diffusion layers (GDLs) utilizing Nafion 111 membrane and Pt/C electrodes with Pt loadings of 0.3 and 0.5 mg_{Pt}/cm² in the anode and cathode, respectively, were used in this study. The MEA and GDL were assembled in the 25 cm² fuel cell testing hardware (Fuel Cell Technologies, Inc.). All fuel cell tests were conducted on a Fuel Cell Test Station (Teledyne Energy System Inc., model 890CL). Cell operation conditions were 65°C

with fully humidified anode and cathode gases at atmospheric pressures. Open-circuit operation for 2 h for cell wet-up were followed by a 25 h MEA conditioning procedure, accomplished by raising the current density and holding for 5 h at 50, 200, 500, 800, and 1000 mA/cm². Following conditioning, the potential of the cell was cycled using a Potentiostat/Galvanostat (EG&G Princeton Applied Research 273A). A square-wave that alternated between 0.87 and 1.2 V vs reference hydrogen electrode (RHE) with a time step 15 s at each potential was used. The anode served as both reference and counter electrodes. The gas flow rates during potential cycling were 0.1 dm³/min (H₂) and 0.3 dm³/min (air or N₂) at the anode and the cathode, respectively. All gas qualities were ultrapure. Electrochemically active surface areas (ECAs) of both electrodes before and after 3000 potential cycles were measured by cyclic voltammetry at a sweep rate of 10 mV/s with 4% H₂ in N₂ (0.1 dm³/min) as reference or counter electrode and sealed deionized water in gas channel of the working electrode. ECA (m²/g_{Pt}) values were calculated by integrating the hydrogen adsorption charge on platinum, which was divided by a value of 210 μC/cm² (assuming hydrogen monolayer adsorption on Pt surface) and further divided by catalyst loading (mg_{Pt}/cm²). Potentiostat control and data acquisition was accomplished with Corware Software 2.8d1 (Scribner Associates Inc.).

Cross sections of a fresh MEA and the potential-cycled MEAs were set in epoxy resin and surface-coated with a uniform thin layer of gold by a gold sputter coater (International Scientific Instruments). A Hitachi S-800 FE SEM equipped with a Kevex EDS detector was used to examine the Pt distribution across these specimens with an acceleration voltage of 15 keV. For each region (anode, cathode, and Pt band), its width (10 tests) and Pt/Au atomic ratio (5 tests) were measured. Overall Pt atom percentages distributed in different regions were estimated by the Pt/Au atomic ratios weighted by the width of the region.

The rate of hydrogen crossover was determined with H₂ at the anode and nitrogen at the cathode under the same fuel cell conditions as those used during potential cycling. A positive potential sweep up to 0.3 V vs OCV (about 0.1 V vs reference hydrogen electrode RHE) was conducted at the cathode with a sweep rate of 1 mV/s. At the end of the sweep, the potential was held constant for 60 s and the limiting oxidation current (mA/cm²) was measured to calculate the H₂ crossover rate (mol/cm²/h). The rate of oxygen crossover in air was measured by gas chromatography (GC) with dry N₂ (0.1 dm³/min) at the anode and 100% RH air (0.3 dm³/min) at the cathode. Both gases were at atmospheric pressure and the cell temperature was 65°C. The oxygen background in pure nitrogen was also tested. Both oxygen and nitrogen calibration curves at proper gas concentration ranges were prepared. Nitrogen effluents at the anode were sampled with a 1 cm³ syringe for GC tests. The oxygen volume percentages in N₂ effluents were determined, which were multiplied by the nitrogen flow rate (0.1 dm³/min) and divided

* Electrochemical Society Student Member.

** Electrochemical Society Active Member.

^z E-mail: wu.bi@chbe.gatech.edu

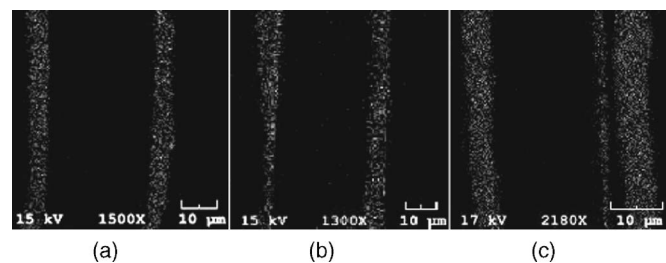


Figure 1. Pt distribution maps in the MEAs (left: anode, right: cathode). (a) Fresh, (b) H_2/N_2 potential cycled, and (c) H_2/air potential cycled.

by MEA area (25 cm^2) to calculate the oxygen crossover rates ($\text{mol}/\text{cm}^2/\text{min}$) using the ideal gas law. Both hydrogen and oxygen crossover tests were repeated three times.

Results and Discussion

For the MEA subjected to H_2/air potential cycling, after conditioning but before cycling, the cathode and the anode had ECAs of 55.4 and $54.2 \text{ m}^2/\text{g}_{Pt}$, respectively. After 3000 H_2/air potential cycles the cathode lost 15.6% of its ECA, whereas the anode had only a 6.3% ECA loss. For the MEA subjected to 3000 H_2/N_2 potential cycles, the cathode and the anode lost 26.3% and 4.4% of their initial ECAs of 53.2 and $54.5 \text{ m}^2/\text{g}_{Pt}$, respectively. The small anode ECA losses may be due to agglomeration of the Pt catalyst by surface diffusion. Pt dissolution is generally believed to be insignificant due to the low potential and the hydrogen reducing environment at the anode.

Figure 1 shows the Pt distributions, determined by SEM-EDS, of a fresh MEA and MEAs after potential cycling. There was no significant Pt found in the membrane for either the fresh MEA or the H_2/N_2 cycled MEA, whereas a clear Pt band formed in the membrane for the H_2/air cycled MEA. These Pt dissolution and deposition behaviors were similar to those found in Yasuda's study.⁸ The regions near the cathode-membrane interface were not examined in this study. Platinum was expected to deposit at the cathode-membrane interface due to the Pt ion reduction by hydrogen from the anode for the H_2/N_2 potential cycling case.

Because there was no element with a constant composition across MEA for reference, the coated Au layers not only provided a better electronic conduction but also functioned as a reference element to quantify the Pt composition in the MEA. The gold layers were assumed perfectly uniform, and both La line peaks of Pt (9.44 keV) and Au (9.71 keV) were selected for Pt/Au atomic ratio determination. The overlap between Pt and Au peaks was small. The average Pt/Au atomic ratios and the widths of the anode, the cathode and the Pt band for the fresh MEA and the potential cycled MEAs are listed in Table I. Following potential cycling, the percentages of the total MEA platinum in the anode (39%) remained very close to the values of the fresh MEA (40%) and to the manufacturer's data (37.5%), suggesting insignificant Pt loss from the anode.

It was found that about $8\%/(8\% + 53\%) \approx 13\%$ Pt (originally in the cathode) deposited in the membrane after 3000 H_2/air potential cycles. Because the width of the Pt band was only about $1.0 \mu\text{m}$

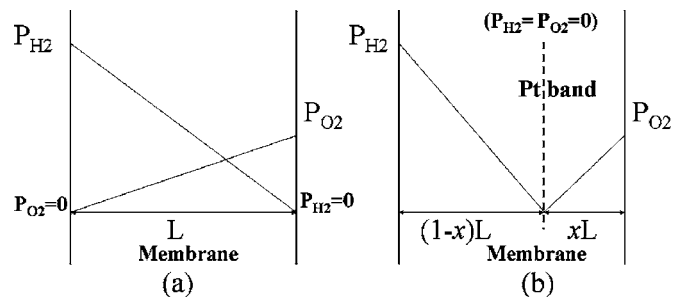


Figure 2. Simplified linear gas pressures profiles of crossover hydrogen and oxygen in membrane (a) before Pt deposition and (b) when Pt-deposited at Pt "band" location.

and the spatial resolution of the SEM-EDS is about $1\text{--}2 \mu\text{m}$, the measured Pt/Au ratios in Pt band may not be very accurate as is evident by the relatively large standard deviation in Table I. But when a Pt band is formed in the membrane, this method is still valuable as a quick and easy estimate of the average cathode Pt loss rate. The Pt loss rate ($3.6 \times 10^{-12} \text{ mol}/\text{cm}^2/\text{s}$ or $2.5 \times 10^{-3} \text{ mg}/\text{cm}^2/\text{h}$) during the total of 3000 potential cycles was about 10 times higher than the dissolution rate of Pt sheet during triangular-wave potential cycling between 0.05 and 1.4 V (vs NHE) at 23°C in 1 M H_2SO_4 .⁴ The ECA loss (15.6%) under H_2/air potential cycling was close to the cathodic Pt loss (13%) to the membrane, but lower than ECA loss (26.3%) under H_2/N_2 potential cycling. This might be caused by the higher Pt surface oxide coverage and lower Pt dissolution rate under the air environment than those in nitrogen at the cathode.¹⁰

The GC tests for oxygen (in air) permeability gave an average crossover rate of $1.3 \pm 0.2 \times 10^{-9} \text{ mol}/\text{cm}^2/\text{s}$. Due to the low detection sensitivity of hydrogen in GC tests, the rate of hydrogen crossover was measured electrochemically, and the average limiting current was $3.10 \pm 0.05 \text{ mA}/\text{cm}^2$. From this the hydrogen crossover rate was calculated to be $1.61 \pm 0.03 \times 10^{-8} \text{ mol}/\text{cm}^2/\text{s}$, which is the same order of magnitude as found in Endoh's study with a Fleming SH50 membrane ($50 \mu\text{m}$ thick).¹¹

Before potential cycling and Pt dissolution, the presumed H_2 and O_2 gas pressure profiles are sketched in Fig. 2a, assuming linear profiles and zero gas pressures at membrane edges due to complete oxygen reduction at the anode and hydrogen oxidation at the cathode. Figure 1c shows that the Pt atoms were deposited in a single thin Pt band instead of being uniformly deposited over a region between the edge of the band and the cathode. We believe that a hydrogen front in membrane (to reduce and deposit Pt ions: Reaction 1) moved from the cathode to the Pt band location during potential cycling. This is explained as follows: because the average rate of Pt deposition (or average Pt ion flux) in the membrane was three orders of magnitude lower than the H_2 crossover rate, we propose that hydrogen is consumed predominantly by reaction with oxygen at the deposited Pt, which functions as a catalyst (Reaction 2). Without a catalyst, hydrogen and oxygen will not react with each other at 65°C (much lower than the ignition temperature). However, it was reported that hydrogen catalytic combustion reaction¹² can

Table I. Average Pt/Au ratios and widths of anode, cathode, and Pt "band" and calculated overall Pt% in MEAs.

MEAs	Fresh MEA		H_2/N_2 potential cycled MEA		H_2/air potential cycled MEA		
	Anode	Cathode	Anode	Cathode	Anode	Cathode	Pt band
Pt/Au ratio	4.0 ± 0.5	4.3 ± 0.3	5.5 ± 0.3	6.1 ± 0.5	4.8 ± 0.2	5.0 ± 0.3	5.1 ± 1.2
Width (μm)	5.2 ± 1.2	7.2 ± 1.1	5.1 ± 1.6	7.1 ± 1.0	5.3 ± 0.8	7.0 ± 1.1	1.0 ± 0.1
MEA Pt%	40%	60%	39%	61%	39%	53%	8%

take place at the Pt single crystal even at temperatures as low as 120 K, and H₂ combustion was continuous with water desorption from catalyst surface if temperature was higher than 170 K.¹³ This catalytic combustion of hydrogen and water production in membrane has previously been applied to design a self-humidifying PEM fuel cell.¹⁴ When H₂/air potential cycling starts, some dissolved Pt ions from the cathode diffuse into the membrane and are deposited by hydrogen reduction at locations very close to the cathode. Because oxygen dominated at these locations, hydrogen that diffuses through the membrane would be completely consumed by the catalytic combustion with the deposited Pt catalyst. This permits Pt ions to move further toward the anode in the membrane until they are reduced by the hydrogen diffusing from the anode. Such processes continue with Pt deposition and the hydrogen front moving away from the cathode. When the hydrogen front reaches a position where both hydrogen and oxygen are completely reacted, Pt ions cannot move further toward the anode, and a pseudo-steady-state of Pt deposition and H₂/O₂ catalytic combustion is achieved. At this location, the mixed potential of dissolved H₂/O₂ dramatically decreases from above 0.8 V to below 0.1 V (vs NHE) due to the transition from an oxygen-rich condition to a hydrogen-rich condition, and the deposited Pt should be stable. A simple linear gas profile in membrane is sketched in Fig. 2b showing this state. Finally, as more Pt ions deposit at this location, a Pt “band” forms. We expect that the band width increases slightly as more Pt is deposited and also due to possible small fluctuation of gas partial pressures



Based on the above straightforward Pt ion deposition processes, the Pt band location in the membrane can be predicted in terms of the rates of gas permeation. At steady state and assuming the gas profiles in Fig. 2b, the hydrogen and oxygen fluxes are related

$$N_{\text{H}_2} = -2N_{\text{O}_2} \quad [3]$$

Assuming Fick’s law

$$\frac{D_{\text{H}_2}c_{\text{H}_2}^0}{1-x} = \frac{2D_{\text{O}_2}c_{\text{O}_2}^0}{x} \quad [4]$$

x is the dimensionless distance from the cathode-membrane interface to the center of Pt band, D_{H_2} and D_{O_2} are effective diffusivities of H₂ and O₂ in membrane, and $c_{\text{H}_2}^0$ and $c_{\text{O}_2}^0$ are H₂ and O₂ concentrations at the membrane edge. Based on Henry’s law

$$c_{\text{H}_2}^0 = H_{\text{H}_2}p_{\text{H}_2}^0 \quad [5]$$

and

$$c_{\text{O}_2}^0 = H_{\text{O}_2}p_{\text{O}_2}^0 \quad [6]$$

where H_{H_2} and H_{O_2} are Henry’s constants for H₂ and O₂ in Nafion membrane, and $p_{\text{H}_2}^0$ and $p_{\text{O}_2}^0$ are H₂ and O₂ partial pressures at membrane edges. Combining Eq. 4-6, we have

$$\frac{1}{x} = 1 + \frac{1}{2\alpha} \times \frac{p_{\text{H}_2}^0}{p_{\text{O}_2}^0} \quad [7]$$

where

$$\alpha = \frac{D_{\text{O}_2}H_{\text{O}_2}}{D_{\text{H}_2}H_{\text{H}_2}} \quad [8]$$

Therefore, the position of the Pt band ($1/x$) should vary linearly with the ratio of hydrogen and oxygen partial pressures. α was evaluated by hydrogen and oxygen in air permeability tests in terms of the crossover rates (N'_{H_2} and N'_{O_2}) as

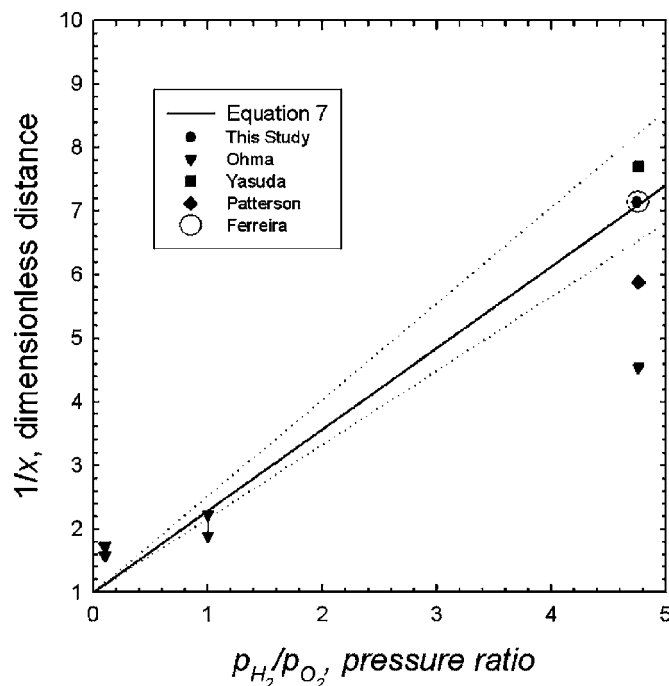


Figure 3. Comparisons of predicted Pt “band” locations with experimental data.

$$\frac{N'_{\text{H}_2}}{N'_{\text{O}_2}} = \frac{D_{\text{H}_2}H_{\text{H}_2}p_{\text{H}_2}^0/L}{D_{\text{O}_2}H_{\text{O}_2}p_{\text{O}_2}^0/L} = \frac{1}{\alpha} \frac{p_{\text{H}_2}^0}{p_{\text{O}_2}^0} \quad [9]$$

α was calculated to be 0.38 ± 0.05 , and therefore the Pt band location x was calculated to be 0.14 by Eq. 7, which was very close to the measured value of 0.15 in SEM-EDS image (Fig. 1c). The predicted Pt band locations and literature data are plotted in Fig. 3. Yasuda’s study⁸ ($x \approx 0.13$) using a Nafion 117 membrane and Ferreira’s study⁷ ($x \approx 0.14$) using a Gore 5510 MEA were very close to the predicted data. The Pt band position in both Patterson’s¹⁵ (Gore MEA) and Ohma’s¹⁶ (Nafion NRE212) studies under H₂/air cases were relatively closer to the anodes than the predicted locations. Ohma’s data showed relatively poor agreement with the predicted results. It seems unlikely, but this may be caused by different permeation rates through the membrane (dissimilar α values). For H₂/N₂ potential cycling (hydrogen/oxygen pressure \rightarrow infinity), the deposition of Pt was expected at the cathode-membrane interface ($1/x \rightarrow$ infinity) because there was no oxygen to suppress hydrogen crossover front.

Pt metal was not observed between the Pt band and the cathode in either this study or Ohma’s study.¹⁶ One possibility was that the Pt atomic concentrations were too low to be detected in SEM and TEM images. Yasuda⁸ believed that nucleation of Pt was not easy under oxygen-rich conditions with a high mixed potential of dissolved hydrogen and oxygen. But Ohma¹⁶ explained that any deposited Pt atoms redissolve at high mixed potential location and the Pt ions move further towards the anode. Further studies that vary oxygen gas pressure during potential cycling are ongoing to check the possibility of the deposited Pt redissolution and Pt band relocation in the membrane. A kinetic model of Pt dissolution and Pt ion deposition in membrane will be built to assist further understanding the Pt deposition mechanisms in membrane.

Conclusions

SEM-EDS analyses using a sample with a uniformly coated thin layer of Au on the surface as a reference provided a simple and effective method for estimating the Pt distribution and for quantifying the amount of Pt deposited in the membrane. For H₂/N₂ potential

cycling deposition of platinum in the membrane was not observed. In contrast, for the case of H₂/air potential cycling, the deposited Pt formed a band in the membrane due to the suppressed hydrogen crossover by H₂/O₂ catalytic combustion reaction on Pt that was deposited in the membrane. The Pt band position was well predicted by a simple model in terms of the rates of hydrogen and oxygen crossover in the membrane separator.

Acknowledgments

This research was financially supported by the Georgia Tech Research Institute, the Hyundai Motors Corporation, and the Ministry of Commerce, Industry and Energy of Korea. The authors also thank to Cheng Chen, Kevin Gallagher, and Rajeswari Chandrasekaran for the discussion of this work.

The Georgia Institute of Technology assisted in meeting the publication costs of this article.

List of Symbols

$c_{\text{H}_2}^0$	H ₂ concentration at membrane/anode interface (mol/m ³)
$c_{\text{O}_2}^0$	O ₂ concentration at membrane/cathode interface (mol/m ³)
D_{H_2}	diffusivity of H ₂ in membrane (m ² /s)
D_{O_2}	diffusivity of O ₂ in membrane (m ² /s)
H_{H_2}	Henry's constant of H ₂ in Nafion membrane (mol/m ³ /Pa)
H_{O_2}	Henry's constant of O ₂ in Nafion membrane (mol/m ³ /Pa)
L	membrane thickness (m)
N_{H_2}	hydrogen crossover flux during fuel cell potential cycling (mol/m ² /s)
N_{O_2}	oxygen crossover flux during fuel cell potential cycling (mol/m ² /s)

N'_{H_2}	hydrogen crossover flux in crossover test (mol/m ² /s)
N'_{O_2}	oxygen in air crossover flux in crossover test (mol/m ² /s)
$P_{\text{H}_2}^0$	H ₂ gas pressure in bulk (76.0 kPa in this study)
$P_{\text{O}_2}^0$	O ₂ gas pressure in bulk (16.0 kPa in this study)
x	dimensionless distance of Pt "band" from cathode
α	ratio of hydrogen and oxygen permeability

References

1. M. Pourbaix, *Atlas of Electrochemical Equilibria in Aqueous Solution*, p. 380, Pergamon Press, Oxford (1966).
2. D. C. Johnson, D. T. Napp, and S. Brunckenstein, *Electrochim. Acta*, **15**, 1493 (1970).
3. D. A. J. Rand and R. Woods, *J. Electroanal. Chem. Interfacial Electrochem.*, **35**, 209 (1972).
4. K. Kinoshita, J. T. Lunquist, and P. Stonehart, *J. Electroanal. Chem. Interfacial Electrochem.*, **48**, 157 (1973).
5. R. M. Darling and J. P. Meyers, *J. Electrochem. Soc.*, **150**, A1523 (2003).
6. R. M. Darling and J. P. Meyers, *J. Electrochem. Soc.*, **152**, A242 (2005).
7. P. J. Ferreira, G. J. la O', Y. Shao-Horn, D. Morgan, R. Makharia, S. Kocha, and H. A. Gasteiger, *J. Electrochem. Soc.*, **152**, A2256 (2005).
8. K. Yasuda, A. Taniguchi, T. Akita, T. Ioroi, and Z. Siroma, *Phys. Chem. Chem. Phys.*, **8**, 746 (2006).
9. P. Yu, M. Pemberton, and P. Plasse, *J. Power Sources*, **144**, 11 (2005).
10. H. Xu, R. Kunz, and J. M. Fenton, *Electrochem. Solid-State Lett.*, **10**, B1 (2007).
11. E. Endoh, S. Terazono, H. Widjaja, and Y. Takimoto, *Electrochem. Solid-State Lett.*, **7**, A209 (2004).
12. G. B. Fisher, J. L. Gland, and S. J. Schmieg, *J. Vac. Sci. Technol.*, **20**, 518 (1982).
13. G. B. Fisher and J. L. Gland, *Surf. Sci.*, **94**, 446 (1980).
14. M. Watanabe, H. Uchida, Y. Seki, M. Emori, and P. Stonehart, *J. Electrochem. Soc.*, **143**, 3847 (1996).
15. (a) T. Patterson, in *Fuel Cell Technology Topical Conference Proceedings*, AIChE (2002); (b) Personal communication.
16. A. Ohma, S. Suga, S. Yamamoto, and K. Shinohara, *ECS Transactions*, **3**(1), 519 (2006).